# Ranking Love Numbers for the Neutron Star Equation of State: The Need for Third-Generation Detectors

Costantino Pacilio,[1,2] Andrea Maselli,[3,4] Margherita Fasano,[1] and Paolo Pani[1,2]
[1]*Dipartimento di Fisica, "Sapienza" Università di Roma, Piazzale Aldo Moro 5, 00185 Roma, Italy*
[2]*INFN, Sezione di Roma, Piazzale Aldo Moro 2, 00185 Roma, Italy*
[3]*Gran Sasso Science Institute (GSSI), I-67100 L'Aquila, Italy*
[4]*INFN, Laboratori Nazionali del Gran Sasso, I-67100 Assergi, Italy*

(Received 26 April 2021; revised 22 January 2022; accepted 10 February 2022; published 10 March 2022)

Gravitational-wave measurements of the tidal deformability in neutron-star binary coalescences can be used to infer the still unknown equation of state (EOS) of dense matter above the nuclear saturation density. By employing a Bayesian-ranking test, we quantify the ability of current and future gravitational-wave observations to discriminate among families of nuclear-physics based EOS which differ in particle content and *ab initio* microscopic calculations. While the constraining power of GW170817 is limited, we show that even twenty coalescences detected by LIGO-Virgo at design sensitivity are not enough to discriminate between EOS with similar softness but distinct microphysics. However, just a single detection with a third-generation detector such as the Einstein Telescope or Cosmic Explorer will rule out several families of EOS with very strong statistical significance and can discriminate among models which feature similar softness, hence, constraining the properties of nuclear matter to unprecedented levels.

DOI: 10.1103/PhysRevLett.128.101101

*Introduction.*—The equation of state (EOS) of dense matter plays a crucial role in many astrophysical phenomena associated with neutron stars (NSs) in different environments and dynamical regimes [1]. The electromagnetic (EM) and gravitational-wave (GW) signals emitted by isolated and (coalescing) binary NSs depend on the properties of the stellar structure and carry precious information on the nature of stellar cores where the density is much larger than the nuclear saturation point, $\rho_0 \approx 2.7 \times 10^{14}$ g/cm$^3$ [2,3]. In this regime, EOS models feature large uncertainties due to the complexity in describing strong interactions at densities where constituents other than nucleons may appear. This uncertainty reflects into a plethora of models with different particle content, featuring, for example, plain $npe\mu$ matter, hyperons, pion condensates, quarks, etc. [2] and, also, predicting different macroscopic stellar properties, such as maximum mass, compactness, and tidal deformability [3–5]. This variety hampers our ability to uniquely characterize the behavior of nuclear matter in extreme conditions and, hence, the NS structure.

Constraints on the EOS in the laboratory are limited by the density regime achievable by terrestrial experiments [6–13]. Major advances are expected to come from astrophysical observations, either from mass-radius measurements in the EM band [1,14–21] or, more recently, from GW observations of binary NS mergers [22–25], where the EOS leaves an imprint in the latest stages of the inspiral and in the post-merger signal. GW measurements of the tidal deformability of coalescing NS binaries [26,27] provide a new tool to probe the behavior of matter at densities above $\rho_0$ [22,28–39] (see [5,40] for recent reviews). The landmark detection of GW170817 has already ruled out very stiff EOS which predict large tidal deformabilities [22,23]. Moreover, the detection of an EM counterpart to GW170817 has motivated several multimessenger analyses aimed at providing joint GW-EM constraints [41–63] (see [3,5,64] for some reviews).

The majority of these approaches interpreted constraints on the tidal deformability using phenomenological EOS, which map wide samples of models in terms of a relatively small set of parameters [65–71], or synthetic EOS [72]. While flexible, these models lack the description of the microphysical content which, otherwise, characterizes *ab initio*, nuclear-physics based EOS. In this Letter, we pursue a complementary approach and try to answer the following question: given a set of nuclear-physics based cold EOS—which differ in the particle content and in the *ab initio* microscopic calculations—what is the one that is mostly favored (in a rigorous statistical sense) by current and future observations?

In order to address this problem, we perform a hierarchical Bayesian test that—given a set of GW data on the binary masses and tidal deformability—ranks different models of dense matter according to their statistical evidence. First, we apply this method to the real data of GW170817, confirming that the constraining power of this event is limited to excluding only very stiff EOS [73]. Then, we extend this approach to a near-future scenario, using current interferometers at design sensitivity and stacking multiple binary NS observations characterized by different masses and distances [38,39]. Our results show that the sensitivity of the advanced LIGO-Virgo interferometers is not sufficient to resolve the degeneracy between EOS featuring similar softness. Therefore, we apply, for the first time, this Bayesian analysis to the Einstein Telescope (ET), a proposed third-generation ground-based GW observatory [74–80]. In this case, we found that even a single ordinary detection would rule out several classes of EOS and is sufficient to discriminate among nuclear-matter models with similar softness. Furthermore, just stacking a few detections would be sufficient to pinpoint a single EOS with decisive statistical evidence.

*EOS catalog and dataset simulations.*—We consider 12 state-of-the-art EOS which can be classified into three broad families depending on their matter content: (i) plain $npe\mu$ nuclear matter—APR3, APR4, SLY, MPA1, MS1, MS1b, WFF1, WFF2 [81–85]; (ii) models with hyperons—GNH3, H4 [86,87]; and (iii) hybrid EOS with mixtures of nucleonic and quark matter—ALF2, SQM3 [88,89]. Naming conventions follow [3,90]. This ensemble of EOS encompasses a wide range of stiffness. For a reference mass $M = 1.4\ M_\odot$, they predict compactness in the range $\mathcal{C} = M/R \in (0.14, 0.20)$ and dimensionless tidal deformabilities in the range $\Lambda \in (151, 1377)$, see Fig. 1 and Table I.

The EOS have been selected to be compatible with J0740 + 6620 [91], the most massive pulsar observed to date ($M = 2.08^{+0.07}_{-0.07}\ M_\odot$ at 68.3% confidence level). In particular, all the considered EOS have a maximum mass above the ($2\sigma$) lower bound 1.94 $M_\odot$ and subluminal sound speed in the relevant mass range. For some EOS, this restricts the range of allowed configurations (e.g., WFF1 marginally satisfies the causality condition).

Besides analyzing the single GW170817 binary NS event, we simulate two selected catalogs of binary NS events consisting of 20 GW sources (see Supplemental Material [93]). The selected masses are drawn uniformly within $(1.2, 1.6)\ M_\odot$, which is compatible with the mass range inferred for GW170817, and luminosity distance $d_L$ drawn uniformly in comoving volume with $60 \leq d_L/\mathrm{Mpc} \leq 210$. We emphasize that, given the large number of binary-NS events expected in the third-generation era [94], one can restrict to a subset of optimal observations, e.g., including only the loudest events with relatively small component masses, which provide the best constraints on the EOS. The injected signals in the two catalogs assume the EOS APR4 and ALF2, respectively, as prototypes of soft and stiff nuclear matter.

We use the `IMRPhenomPv2_NRTidal` model [95,96] GW waveform template. We inject nonspinning binaries, and we recover the component spins imposing a low-spin prior $\chi_{1,2} \in [-0.05, 0.05]$ and assuming spins are (anti-)aligned. To help comparison between the events, we fix the same sky location and inclination for all sources, avoiding particularly optimistic or pessimistic choices. We inject 64-second long waveforms into a zero-noise configuration as described in [97], either for a network composed by the LIGO Hanford, LIGO Livingston, and Virgo detectors at design sensitivity [98], or for the future third-generation interferometer Einstein Telescope in its ET-D configuration [78]. We checked that our results also

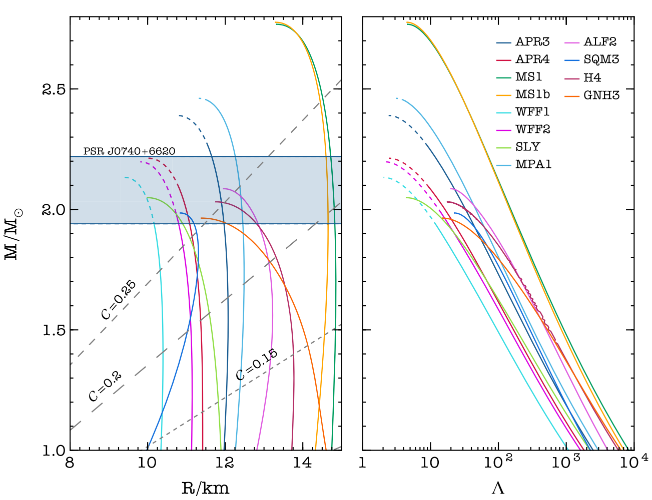


FIG. 1. Mass-radius and mass-tidal deformability diagrams for the EOS considered in the Bayesian analysis. The blue band on the left panel corresponds to the most massive pulsar observed in the EM band ($M = 2.08^{+0.07}_{-0.07}\ M_\odot$ [91]), while dashed lines identify configurations with fixed compactness $\mathcal{C} = M/R$. Solid (dashed) curves correspond to stellar configurations with the speed of sound at the center smaller (larger) than the speed of light.

TABLE I. List of the selected EOS with the corresponding calculation methods (family), particle content, and dimensionless tidal deformability at the reference mass $M = 1.4\ M_\odot$. The families are distinguished in: nuclear many body (nmbt) calculations and mean-field theory (mft) (see [92] for a review on EOS calculations). In the ALF2 and SQM3 EOS the quark ($Q$) content is modelled according to the MIT bag model, while the GNH3, H4, and SQM3 EOS include hyperons ($H$).

| EOS | Family | Particles | $\Lambda_{1.4}$ |
|---|---|---|---|
| ALF2 | nmbt + bag | $npe\mu + Q$ | 754 |
| APR3 | nmbt | $npe\mu$ | 390 |
| APR4 | nmbt | $npe\mu$ | 261 |
| GNH3 | mft | $npe\mu + H$ | 866 |
| H4 | mft | $npe\mu + H$ | 897 |
| MPA1 | mft | $npe\mu$ | 487 |
| MS1 | mft | $npe\mu$ | 1377 |
| MS1b | mft | $npe\mu$ | 1250 |
| SLY | mft | $npe\mu$ | 297 |
| SQM3 | mft + bag | $npe\mu + H + Q$ | 432 |
| WFF1 | nmbt | $npe\mu$ | 151 |
| WFF2 | nmbt | $npe\mu$ | 229 |

remain valid when using a random realization of the detector noise.

For a given simulated observation, we reconstruct the posterior probability distribution of the waveform parameters using the publicly available BILBY code, a Bayesian inference library for GW astronomy [99,100]. We use analytic marginalization procedures for the binary orbital phase, luminosity distance, and time of coalescence, as described in [100]. We marginalize on the inferred posterior probability distribution to extract the joint probability function $\mathcal{P}(\mathcal{M}, \eta, \tilde{\Lambda})$ for the binary chirp mass $\mathcal{M}$, symmetric mass ratio $\eta$, and effective tidal deformability [26]

$$\tilde{\Lambda} = \frac{16}{13}\left[\frac{(m_1 + 12m_2)m_1^4\Lambda_1}{(m_1 + m_2)^5} + 1 \leftrightarrow 2\right]. \tag{1}$$

For a given EOS, $\tilde{\Lambda}$ depends only on the two source-frame masses $m_1$ and $m_2$ or, equivalently, on $\mathcal{M}$ and $\eta$.

*Bayesian methods.*—Given the data $\mathcal{D}$ from a GW event compatible with a coalescing NS binary, the degree of belief that the two NSs obey a given EOS can be quantified by the evidence [50]

$$\mathcal{Z}(\mathcal{D}|\mathrm{EOS}) = \int_a^b dp^{(1)} \int_a^b dp^{(2)} \mathcal{P}(\mathcal{M}, \eta, \tilde{\Lambda}|\mathcal{D}) \times \mathcal{P}(p^{(1)}|\mathrm{EOS})\mathcal{P}(p^{(2)}|\mathrm{EOS}), \tag{2}$$

where $p^{(1)}$ and $p^{(2)}$ are the central pressures of the two NSs. For any given EOS, there is a deterministic mapping between the central pressures and the waveform parameters, $\{p^{(1)}, p^{(2)}\} \to \{\mathcal{M}, \eta, \tilde{\Lambda}\}$, and in the above equation, $\{\mathcal{M}, \eta, \tilde{\Lambda}\}$ are evaluated as functions of $\{p^{(1)}, p^{(2)}\}$.

The priors on the central pressures are uniform distributions within $p^{(i)} \in [a, b]$, where $a = p_{\min} \simeq 1.21 \times 10^{34}$ dyne/cm$^2$ and $b = p_{\max}$ corresponds, for a given EOS, to the value of the pressure which yields the maximum mass configuration compatible with causality.

The calculation of the evidence in Eq. (2) can be largely simplified using the fact that the chirp mass of NS binaries is measured with exquisite precision [97], since these sources perform several cycles in band. (For example, the chirp mass of GW170817 was measured with $\approx 0.1\%$ precision, much better than any other intrinsic parameter [22].) Therefore, in Eq. (2), we can fix $\mathcal{M}$ to its median inferred value $\mathcal{M}_\star$. Note that an accurate measurement of the source-frame masses solely from GWs can be hindered by the well-known degeneracy between the inclination angle and the luminosity distance [101,102], which may induce potential biases in the redshift measurement. To resolve this degeneracy, we assume that the redshift of the selected events is known (e.g., if independently measured by an EM counterpart as in GW170817 [23]). Thus, we fix $\mathcal{M}_\star = \mathcal{M}_\star^{\mathrm{det}}/(1+z)$, where $\mathcal{M}_\star^{\mathrm{det}}$ is the median of the inferred distribution of the detector-frame chirp mass, and $z$ is the injected value of the redshift. We also verified that our analysis is not significantly affected by shifting $z$ away from its injected value by $\pm 10\%$, which is very conservative since it corresponds to the accuracy in $z$ as measured from the GW170817 EM counterpart [23].

Following [50], the conditional probability $\mathcal{P}(\eta, \tilde{\Lambda}|\mathcal{M}_\star, \mathcal{D})$ can be replaced by the marginalized probability $\mathcal{P}(\eta, \tilde{\Lambda}|\mathcal{D})$ to a very good approximation, and the evidence reduces to

$$\mathcal{Z}(\mathcal{D}|\mathrm{EOS}) = \int_a^b dp^{(1)} \mathcal{P}\left(\eta(p^{(1)}, p_\star^{(2)}), \tilde{\Lambda}(p^{(1)}, p_\star^{(2)})|\mathcal{D}\right) \times \mathcal{P}(p^{(1)}|\mathrm{EOS})\mathcal{P}(p_\star^{(2)}|\mathrm{EOS}), \tag{3}$$

where $p_\star^{(2)}$ is the solution (if it exists) of $\mathcal{M}(p^{(1)}, p_\star^{(2)}) = \mathcal{M}_\star$. The above equations assume that the EOS configurations are sampled uniformly with respect to the central pressures. However, one could have equally used any monotonic function of the pressure. In particular, we opt for sampling the EOS uniformly with respect to $\log_{10}(p^{(1)})$ and change the integral in Eq. (3) accordingly.

We can use the Bayes factor,

$$\mathcal{B}_2^1 = \frac{\mathcal{Z}(\mathcal{D}|\mathrm{EOS}_1)}{\mathcal{Z}(\mathcal{D}|\mathrm{EOS}_2)}, \tag{4}$$

to express the relative odds of two EOS given the data $\mathcal{D}$, assuming equal priors on the EOS, $\mathcal{P}(\mathrm{EOS}_1) = \mathcal{P}(\mathrm{EOS}_2)$.

The previous discussion can be easily extended to the case of stacked observations $\vec{\mathcal{D}} = \{\mathcal{D}_1 \ldots \mathcal{D}_n\}$. After $n$ observations, the relative odds will be updated by the cumulative Bayes factor

$$\mathcal{B}_2^1 = \prod_{k=1}^{n} \frac{\mathcal{Z}(\mathcal{D}_k|\mathrm{EOS}_1)}{\mathcal{Z}(\mathcal{D}_k|\mathrm{EOS}_2)}. \tag{5}$$

The main quantity of interest is the cumulative logarithmic Bayes factor, $\log_{10} \mathcal{B}_T^i$, between a candidate $\mathrm{EOS}_i$ and a benchmark $\mathrm{EOS}_T$ after $n$ GW detections. We adopt the Kass-Raftery criterion [103] and decisively exclude $\mathrm{EOS}_i$ with respect to $\mathrm{EOS}_T$ when $\log_{10} \mathcal{B}_T^i < -2$.

*Results.*—We start by applying this method to real data, using GW170817 [22,23], the only binary NS GW event—among those detected so far by LIGO and Virgo [104,105]—that provided an accurate measurement of the tidal deformability [23,106]. Figure 2 shows the Bayes factors of different EOS in the catalog normalized with respect to the EOS with maximum evidence, which turns out to be WFF2. The evidence against other EOS is weak in most cases, except for GNH3 and H4, and especially for MS1 and MS1b which are decisively excluded according to the Kass-Raftery scale. This is in agreement with the fact that MS1 and MS1b are the stiffest

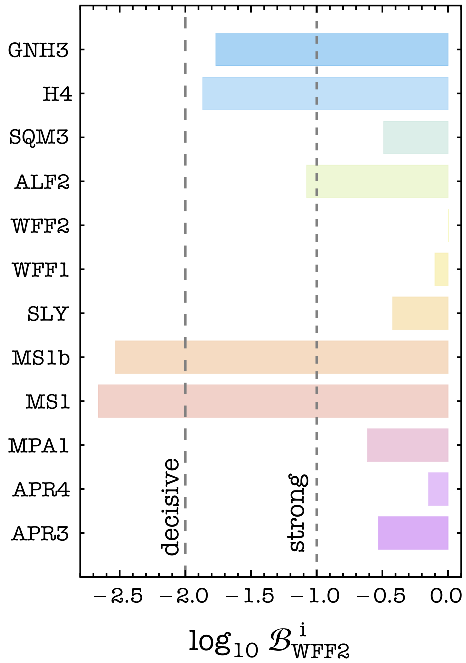


FIG. 2. Bayes factors for different EOS models computed for GW170817 and normalized with respect to the EOS with maximum evidence in the catalog (WFF2). Vertical dashed lines identify the threshold above which the Bayes factor provides a strong and decisive evidence in favor of WFF2.

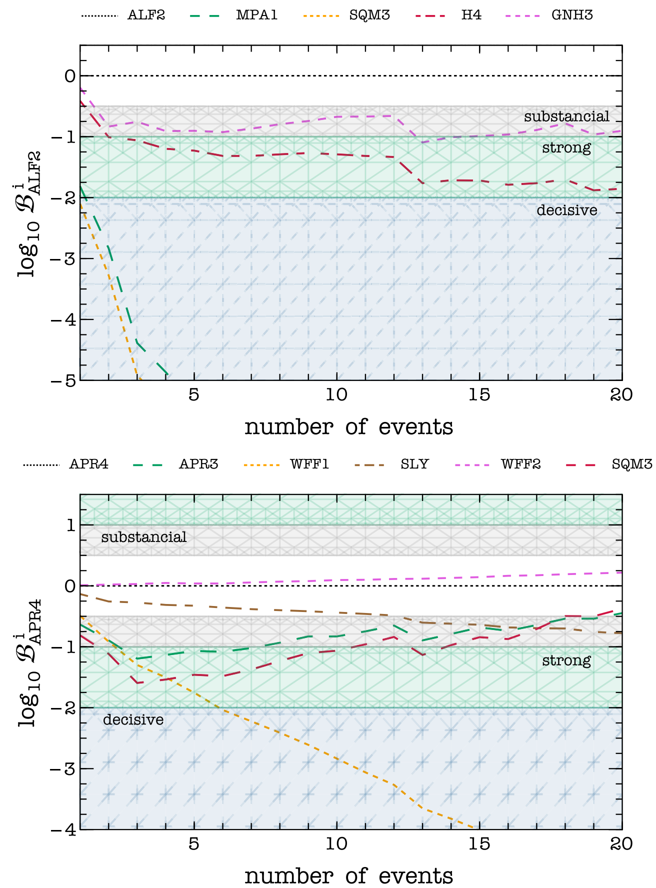


FIG. 3. Evolution of the EOS Bayes factor with the number of events for the LIGO-Virgo network at design sensitivity. Top and bottom panels refer to the ALF2 (stiff EOS) and AP4 (soft EOS) injections, respectively. In each panel, the quantity $\log_{10} \mathcal{B}^i_T$ is normalized with respect to the injected EOS. Shaded bands mark the boundaries of the evidence criteria according to the Kass-Raftery scale [103]. In particular, $\log_{10} \mathcal{B}^i_T < -2$ indicates decisive unfavorable evidence.

EOS in our catalog and, therefore, the easiest to rule out with GW170817 [23,41,44,46,48,73,106,107]. Likewise, EOS stiffer than MS1 and MS1b are even more disfavored by GW170817.

Stronger constraints and statistical evidence can be obtained from accumulating more detections [38,39]. In Fig. 3, we show the Bayes factor as a function of the number of randomly chosen events detected by the advanced LIGO-Virgo network at design sensitivity and assuming the real EOS is either: (i) relatively stiff (ALF2, top panel) or (ii) relatively soft (APR4, bottom panel). In each panel, we show only the subset of EOS with the highest Bayes factors, whereas the other EOS are easier to rule out. In both cases, it is challenging to rule out EOS with stiffness similar to the reference one even after 20 detections (this is more evident for a soft model such as APR4, shown in the bottom panel). This analysis shows, in a clear and statistically robust way, that while several LIGO-Virgo detections at design sensitivity could discriminate among some stiff EOS (e.g., ALF2 versus MPA1 and SQM3) and between some soft and stiff models [38], they remain inconclusive, since the sensitivity is not enough to discriminate among wide classes of EOS with similar stiffness.

The latter conclusion motivates us to forecast a similar analysis in the era of third-generation GW detectors [74–80]. The situation here drastically changes, as shown in Fig. 4. We simulated the same 20 detections with ET, by assuming the conservative case of an underlying APR4 EOS, as in the bottom panel of Fig. 3. For each event, we plot the Bayes factors normalized by the injected EOS, and we only show those EOS which have nonvanishing evidence ($\log_{10} \mathcal{B}^i_{\mathrm{APR4}} > -10$) for at least one event. The fact that most EOS have negligible evidence is a consequence of the much higher sensitivity of the ET detector, and it allows us to exclude all but a couple of EOS of our dataset (namely WFF2 and SLY, which feature a tidal deformability similar to APR4) with only a single observation.

Even in the most pessimistic case, in which a single observation is not enough to exclude a given EOS, stacking two or three detections would allow us to decisively exclude all EOS in the catalog other than the reference one. Even stronger conclusions apply to the case in which the reference EOS are stiff (as for ALF2): in this case, all the other EOS in our catalog are decisively excluded for any single event.

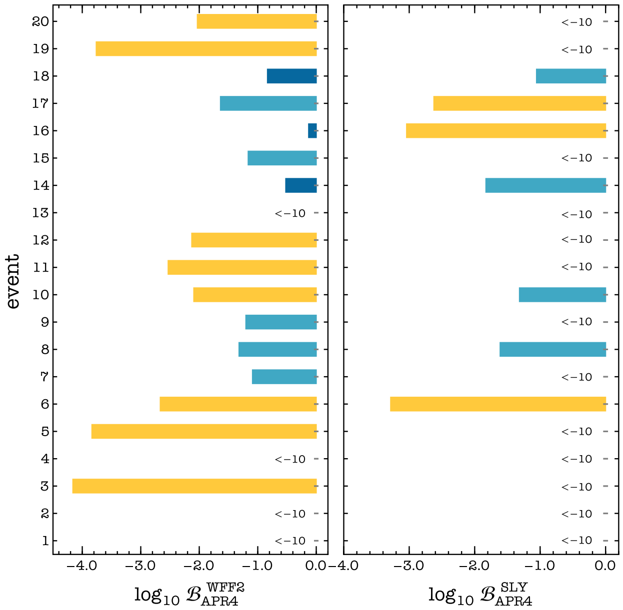


FIG. 4. Bayes factors for simulated observations with ET, relative to the injected EOS APR4, for WFF2 and SLY. The remaining set of ten EOS yield $\log_{10} \mathcal{B}^{i}_{\rm APR4} < -10$ for all events, and they are not shown in the plot.

Thus, at variance with advanced LIGO-Virgo, ET will be able to distinguish among EOS with similar softness and, also, among EOS families featuring different microphysical properties (see Table I). For example, a single ET detection of any of the 20 events considered in our catalog would be sufficient to exclude APR3 relative to APR4 ($\log_{10} \mathcal{B}^{\rm APR3}_{\rm APR4} < -10$). These two EOS feature the same particle content but differ in the description of the nucleon interaction.

*Conclusions.—*We proposed a robust Bayesian-ranking test to discriminate among families of *ab initio* nuclear EOS using GW observations. We applied this test to GW170817, which very mildly favors a relatively soft, standard $npe\mu$ EOS (WFF2), although its power in ruling out EOS with similar stiffness is limited. Furthermore, we showed that near-future observations will not be conclusive: even 20 NS binary detections with LIGO-Virgo at design sensitivity will not be able to distinguish among well-motivated nuclear models.

On the other hand, a single detection by ET will rule out with decisive statistical evidence most of the EOS, including those with comparable softness. In addition, just a few combined detections can be sufficient to robustly identify the best-fit EOS within a catalog, hence, constraining the particle content of nuclear matter at ultrahigh density. The same conclusion would apply assuming that binaries are observed by the proposed Cosmic Explorer [76,77], which features a noise curve similar to that of ET-D at high frequencies, where tidal effects contribute more to the GW signal. Joint detections by ET and Cosmic Explorer would further strengthen our results.

Measuring the masses and tidal deformabilities from multiple events would allow us to quantify the faithfulness of the best-fit EOS, e.g., by looking for inconsistencies between the best-fit predictions and the data in the $\Lambda - M$ plane (see Fig. 1), in case the "true" EOS is not in the dataset.

A further advantage of our approach based on a ranking test among nuclear-physics based EOS is that it can be straightforwardly extended to accommodate other measurements by combining the likelihoods of different models. It would be interesting to extend our analysis in this direction by combining future GW observations with EM ones [50,59], or with post-merger signals [25].

We are indebted to Swetha Bhagwat, Omar Benhar, Marica Branchesi, and Valeria Ferrari for discussions and comments on the manuscript. Numerical calculations have been made possible through a CINECA-INFN agreement, providing access to resources on MARCONI at CINECA. We acknowledge financial support provided under the European Union's H2020 ERC, Starting Grant Agreement No. DarkGRA–757480. We also acknowledge support under the MIUR PRIN and FARE Programmes (GW-NEXT, Grant No. CUP: B84I20000100001), and from the Amaldi Research Center funded by the MIUR program "Dipartimento di Eccellenza" (Grant No. CUP: B81I18001170001).

[1] F. Ozel, G. Baym, and T. Guver, Astrophysical measurement of the equation of state of neutron star matter, Phys. Rev. D **82**, 101301(R) (2010).

[2] J. M. Lattimer and M. Prakash, Neutron star observations: Prognosis for equation of state constraints, Phys. Rep. **442**, 109 (2007).

[3] F. Özel and P. Freire, Masses, radii, and the equation of state of neutron stars, Annu. Rev. Astron. Astrophys. **54**, 401 (2016).

[4] E. Poisson and C. Will, *Gravity: Newtonian, Post-Newtonian, Relativistic* (Cambridge University Press, Cambridge, England, 2014).

[5] K. Chatziioannou, Neutron star tidal deformability and equation of state constraints, Gen. Relativ. Gravit. **52**, 109 (2020).

[6] B.-A. Li and X. Han, Constraining the neutron–proton effective mass splitting using empirical constraints on the density dependence of nuclear symmetry energy around normal density, Phys. Lett. B **727**, 276 (2013).

[7] P. Russotto *et al.*, Results of the ASY-EOS experiment at GSI: The symmetry energy at suprasaturation density, Phys. Rev. C **94**, 034608 (2016).

[8] M. B. Tsang, Y. Zhang, P. Danielewicz, M. Famiano, Z. Li, W. G. Lynch, and A. W. Steiner, Constraints on the Density Dependence of the Symmetry Energy, Phys. Rev. Lett. **102**, 122701 (2009).

[9] B. A. Brown, Constraints on the Skyrme Equations of State from Properties of Doubly Magic Nuclei, Phys. Rev. Lett. **111**, 232502 (2013).

[10] Z. Zhang and L.-W. Chen, Constraining the symmetry energy at subsaturation densities using isotope binding

energy difference and neutron skin thickness, Phys. Lett. B **726**, 234 (2013).
[11] P. Danielewicz, R. Lacey, and W. G. Lynch, Determination of the equation of state of dense matter, Science **298**, 1592 (2002).
[12] S. Shlomo, V. M. Kolomietz, and G. Colò, Deducing the nuclear-matter incompressibility coefficient from data on isoscalar compression modes, Eur. Phys. J. A **30**, 23 (2006).
[13] G. Colò, The compression modes in atomic nuclei and their relevance for the nuclear equation of state, Phys. Part. Nucl. **39**, 286 (2008).
[14] P. Demorest, T. Pennucci, S. Ransom, M. Roberts, and J. Hessels, Shapiro delay measurement of a two solar mass neutron star, Nature (London) **467**, 1081 (2010).
[15] J. Antoniadis *et al.*, A massive pulsar in a compact relativistic binary, Science **340**, 6131 (2013).
[16] E. Fonseca *et al.*, The NANOGrav nine-year data set: Mass and geometric measurements of binary millisecond pulsars, Astrophys. J. **832**, 167 (2016).
[17] H. T. Cromartie *et al.*, Relativistic Shapiro delay measurements of an extremely massive millisecond pulsar, Nat. Astron. **4**, 72 (2020).
[18] A. W. Steiner, J. M. Lattimer, and E. F. Brown, The equation of state from observed masses and radii of neutron stars, Astrophys. J. **722**, 33 (2010).
[19] T. Guver and F. Ozel, The mass and the radius of the neutron star in the transient low mass x-ray binary SAX J1748.9-2021, Astrophys. J. Lett. **765**, L1 (2013).
[20] T. E. Riley *et al.*, A *NICER* view of PSR J0030 + 0451: Millisecond pulsar parameter estimation, Astrophys. J. Lett. **887**, L21 (2019).
[21] M. Miller *et al.*, PSR J0030 + 0451 mass and radius from *NICER* data and implications for the properties of neutron star matter, Astrophys. J. Lett. **887**, L24 (2019).
[22] B. Abbott *et al.* (LIGO Scientific, Virgo Collaborations), Gw170817: Observation of Gravitational Waves from a Binary Neutron Star Inspiral, Phys. Rev. Lett. **119**, 161101 (2017).
[23] B. Abbott *et al.* (LIGO Scientific, Virgo Collaborations), Properties of the Binary Neutron Star Merger GW170817, Phys. Rev. X **9**, 011001 (2019).
[24] B. Abbott *et al.* (LIGO Scientific, Virgo Collaborations), GW190425: Observation of a compact binary coalescence with total mass $\sim 3.4\ M_{\odot}$, Astrophys. J. Lett. **892**, L3 (2020).
[25] L. Baiotti and L. Rezzolla, Binary neutron star mergers: A review of Einstein's richest laboratory, Rep. Prog. Phys. **80**, 096901 (2017).
[26] E. E. Flanagan and T. Hinderer, Constraining neutron star tidal Love numbers with gravitational wave detectors, Phys. Rev. D **77**, 021502(R) (2008).
[27] T. Hinderer, Tidal Love numbers of neutron stars, Astrophys. J. **677**, 1216 (2008).
[28] T. Hinderer, B. D. Lackey, R. N. Lang, and J. S. Read, Tidal deformability of neutron stars with realistic equations of state and their gravitational wave signatures in binary inspiral, Phys. Rev. D **81**, 123016 (2010).
[29] L. Baiotti, T. Damour, B. Giacomazzo, A. Nagar, and L. Rezzolla, Analytic Modeling of Tidal Effects in the Relativistic Inspiral of Binary Neutron Stars, Phys. Rev. Lett. **105**, 261101 (2010).
[30] L. Baiotti, T. Damour, B. Giacomazzo, A. Nagar, and L. Rezzolla, Accurate numerical simulations of inspiralling binary neutron stars and their comparison with effective-one-body analytical models, Phys. Rev. D **84**, 024017 (2011).
[31] J. Vines, E. E. Flanagan, and T. Hinderer, Post-1-Newtonian tidal effects in the gravitational waveform from binary inspirals, Phys. Rev. D **83**, 084051 (2011).
[32] F. Pannarale, L. Rezzolla, F. Ohme, and J. S. Read, Will black hole-neutron star binary inspirals tell us about the neutron star equation of state?, Phys. Rev. D **84**, 104017 (2011).
[33] J. E. Vines and E. E. Flanagan, Post-1-Newtonian quadrupole tidal interactions in binary systems, Phys. Rev. D **88**, 024046 (2013).
[34] B. D. Lackey, K. Kyutoku, M. Shibata, P. R. Brady, and J. L. Friedman, Extracting equation of state parameters from black hole-neutron star mergers. I. Nonspinning black holes, Phys. Rev. D **85**, 044061 (2012).
[35] A. Maselli, L. Gualtieri, and V. Ferrari, Constraining the equation of state of nuclear matter with gravitational wave observations: Tidal deformability and tidal disruption, Phys. Rev. D **88**, 104040 (2013).
[36] B. D. Lackey, K. Kyutoku, M. Shibata, P. R. Brady, and J. L. Friedman, Extracting equation of state parameters from black hole-neutron star mergers: Aligned-spin black holes and a preliminary waveform model, Phys. Rev. D **89**, 043009 (2014).
[37] M. Favata, Systematic Parameter Errors in Inspiraling Neutron Star Binaries, Phys. Rev. Lett. **112**, 101101 (2014).
[38] W. Del Pozzo, T. G. F. Li, M. Agathos, C. Van Den Broeck, and S. Vitale, Demonstrating the Feasibility of Probing the Neutron Star Equation of State with Second-Generation Gravitational Wave Detectors, Phys. Rev. Lett. **111**, 071101 (2013).
[39] B. D. Lackey and L. Wade, Reconstructing the neutron-star equation of state with gravitational-wave detectors from a realistic population of inspiralling binary neutron stars, Phys. Rev. D **91**, 043002 (2015).
[40] A. Guerra Chaves and T. Hinderer, Probing the equation of state of neutron star matter with gravitational waves from binary inspirals in light of GW170817: A brief review, J. Phys. G **46**, 123002 (2019).
[41] E. Annala, T. Gorda, A. Kurkela, and A. Vuorinen, Gravitational-Wave Constraints on the Neutron-Star-Matter Equation of State, Phys. Rev. Lett. **120**, 172703 (2018).
[42] B. Margalit and B. D. Metzger, Constraining the maximum mass of neutron stars from multi-messenger observations of GW170817, Astrophys. J. Lett. **850**, L19 (2017).
[43] D. Radice, A. Perego, F. Zappa, and S. Bernuzzi, GW170817: Joint constraint on the neutron star equation of state from multimessenger observations, Astrophys. J. Lett. **852**, L29 (2018).
[44] A. Bauswein, O. Just, H.-T. Janka, and N. Stergioulas, Neutron-star radius constraints from GW170817 and future detections, Astrophys. J. Lett. **850**, L34 (2017).
[45] Y. Lim and J. W. Holt, Neutron Star Tidal Deformabilities Constrained by Nuclear Theory and Experiment, Phys. Rev. Lett. **121**, 062701 (2018).

[46] E. R. Most, L. R. Weih, L. Rezzolla, and J. Schaffner-Bielich, New Constraints on Radii and Tidal Deformabilities of Neutron Stars from GW170817, Phys. Rev. Lett. **120**, 261103 (2018).

[47] Z. Carson, A. W. Steiner, and K. Yagi, Constraining nuclear matter parameters with GW170817, Phys. Rev. D **99**, 043010 (2019).

[48] S. De, D. Finstad, J. M. Lattimer, D. A. Brown, E. Berger, and C. M. Biwer, Tidal Deformabilities and Radii of Neutron Stars from the Observation of GW170817, Phys. Rev. Lett. **121**, 091102 (2018); Erratum, Phys. Rev. Lett. **121**, 259902 (2018).

[49] E. Annala, T. Gorda, A. Kurkela, J. Nättilä, and A. Vuorinen, Evidence for quark-matter cores in massive neutron stars, Nat. Phys. **16**, 907 (2020).

[50] G. Raaijmakers *et al.*, Constraining the dense matter equation of state with joint analysis of NICER and LIGO/Virgo measurements, Astrophys. J. Lett. **893**, L21 (2020).

[51] C. D. Capano, I. Tews, S. M. Brown, B. Margalit, S. De, S. Kumar, D. A. Brown, B. Krishnan, and S. Reddy, Stringent constraints on neutron-star radii from multimessenger observations and nuclear theory, Nat. Astron. **4**, 625 (2020).

[52] M. C. Miller, C. Chirenti, and F. K. Lamb, Constraining the equation of state of high-density cold matter using nuclear and astronomical measurements, Astrophys. J. **888**, 12 (2020).

[53] B. Kumar and P. Landry, Inferring neutron star properties from GW170817 with universal relations, Phys. Rev. D **99**, 123026 (2019).

[54] M. Fasano, T. Abdelsalhin, A. Maselli, and V. Ferrari, Constraining the Neutron Star Equation of State Using Multiband Independent Measurements of Radii and Tidal Deformabilities, Phys. Rev. Lett. **123**, 141101 (2019).

[55] H. Güven, K. Bozkurt, E. Khan, and J. Margueron, Multimessenger and multiphysics Bayesian inference for GW170817 binary neutron star merger, Phys. Rev. C **102**, 015805 (2020).

[56] S. Traversi, P. Char, and G. Pagliara, Bayesian inference of dense matter equation of state within relativistic mean field models using astrophysical measurements, Astrophys. J. **897**, 165 (2020).

[57] P. Landry, R. Essick, and K. Chatziioannou, Nonparametric constraints on neutron star matter with existing and upcoming gravitational wave and pulsar observations, Phys. Rev. D **101**, 123007 (2020).

[58] T. Dietrich, M. W. Coughlin, P. T. H. Pang, M. Bulla, J. Heinzel, L. Issa, I. Tews, and S. Antier, Multimessenger constraints on the neutron-star equation of state and the Hubble constant, Science **370**, 1450 (2020).

[59] J. Zimmerman, Z. Carson, K. Schumacher, A. W. Steiner, and K. Yagi, Measuring nuclear matter parameters with NICER and LIGO/Virgo, arXiv:2002.03210.

[60] H. O. Silva, A. M. Holgado, A. Cárdenas-Avendaño, and N. Yunes, Astrophysical and Theoretical Physics Implications from Multimessenger Neutron Star Observations, Phys. Rev. Lett. **126**, 181101 (2021).

[61] M. Al-Mamun, A. W. Steiner, J. Nättilä, J. Lange, R. O'Shaughnessy, I. Tews, S. Gandolfi, C. Heinke, and S. Han, Combining Electromagnetic and Gravitational-Wave Constraints on Neutron-Star Masses and Radii, Phys. Rev. Lett. **126**, 061101 (2021).

[62] A. Sabatucci and O. Benhar, Tidal deformation of neutron stars from microscopic models of nuclear dynamics, Phys. Rev. C **101**, 045807 (2020).

[63] A. Maselli, A. Sabatucci, and O. Benhar, Constraining three-nucleon forces with multimessenger data, Phys. Rev. C **103**, 065804 (2021).

[64] L. Baiotti, Gravitational waves from neutron star mergers and their relation to the nuclear equation of state, Prog. Part. Nucl. Phys. **109**, 103714 (2019).

[65] J. S. Read, B. D. Lackey, B. J. Owen, and J. L. Friedman, Constraints on a phenomenologically parametrized neutron-star equation of state, Phys. Rev. D **79**, 124032 (2009).

[66] L. Lindblom, Spectral representations of neutron-star equations of state, Phys. Rev. D **82**, 103011 (2010).

[67] K. Hebeler, J. M. Lattimer, C. J. Pethick, and A. Schwenk, Equation of state and neutron star properties constrained by nuclear physics and observation, Astrophys. J. **773**, 11 (2013).

[68] S. K. Greif, G. Raaijmakers, K. Hebeler, A. Schwenk, and A. L. Watts, Equation of state sensitivities when inferring neutron star and dense matter properties, Mon. Not. R. Astron. Soc. **485**, 5363 (2019).

[69] K. Hebeler, J. D. Holt, J. Menendez, and A. Schwenk, Nuclear forces and their impact on neutron-rich nuclei and neutron-rich matter, Annu. Rev. Nucl. Part. Sci. **65**, 457 (2015).

[70] I. Tews, J. Carlson, S. Gandolfi, and S. Reddy, Constraining the speed of sound inside neutron stars with chiral effective field theory interactions and observations, Astrophys. J. **860**, 149 (2018).

[71] B. Biswas, P. Char, R. Nandi, and S. Bose, Towards mitigation of apparent tension between nuclear physics and astrophysical observations by improved modeling of neutron star matter, Phys. Rev. D **103**, 103015 (2021).

[72] P. Landry and R. Essick, Nonparametric inference of the neutron star equation of state from gravitational wave observations, Phys. Rev. D **99**, 084049 (2019).

[73] B. P. Abbott *et al.* (LIGO Scientific, Virgo Collaborations), Model comparison from LIGO–Virgo data on GW170817's binary components and consequences for the merger remnant, Classical Quant. Grav. **37**, 045006 (2020).

[74] M. Punturo *et al.*, The Einstein Telescope: A third-generation gravitational wave observatory, Classical Quant. Grav. **27**, 194002 (2010).

[75] S. Dwyer, D. Sigg, S. W. Ballmer, L. Barsotti, N. Mavalvala, and M. Evans, Gravitational wave detector with cosmological reach, Phys. Rev. D **91**, 082001 (2015).

[76] B. P. Abbott *et al.* (LIGO Scientific Collaboration), Exploring the sensitivity of next generation gravitational wave detectors, Classical Quant. Grav. **34**, 044001 (2017).

[77] R. Essick, S. Vitale, and M. Evans, Frequency-dependent responses in third generation gravitational-wave detectors, Phys. Rev. D **96**, 084004 (2017).

[78] S. Hild *et al.*, Sensitivity studies for third-generation gravitational wave observatories, Classical Quant. Grav. **28**, 094013 (2011).

[79] B. S. Sathyaprakash *et al.*, Extreme gravity and fundamental physics, arXiv:1903.09221.

[80] M. Maggiore *et al.*, Science case for the Einstein Telescope, J. Cosmol. Astropart. Phys. 03 (2020) 050.

[81] A. Akmal, V. R. Pandharipande, and D. G. Ravenhall, The equation of state of nucleon matter and neutron star structure, Phys. Rev. C **58**, 1804 (1998).

[82] F. Douchin and P. Haensel, A unified equation of state of dense matter and neutron star structure, Astron. Astrophys. **380**, 151 (2001).

[83] H. Müther, M. Prakash, and T. Ainsworth, The nuclear symmetry energy in relativistic Brueckner-Hartree-Fock calculations, Phys. Lett. B **199**, 469 (1987).

[84] H. Mueller and B. D. Serot, Relativistic mean field theory and the high density nuclear equation of state, Nucl. Phys. **A606**, 508 (1996).

[85] R. B. Wiringa, V. Fiks, and A. Fabrocini, Equation of state for dense nucleon matter, Phys. Rev. C **38**, 1010 (1988).

[86] N. Glendenning, Neutron stars are giant hypernuclei?, Astrophys. J. **293**, 470 (1985).

[87] B. D. Lackey, M. Nayyar, and B. J. Owen, Observational constraints on hyperons in neutron stars, Phys. Rev. D **73**, 024021 (2006).

[88] M. Alford, M. Braby, M. Paris, and S. Reddy, Hybrid stars that masquerade as neutron stars, Astrophys. J. **629**, 969 (2005).

[89] M. Prakash, J. R. Cooke, and J. M. Lattimer, Quark-hadron phase transition in protoneutron stars, Phys. Rev. D **52**, 661 (1995).

[90] J. M. Lattimer and M. Prakash, Neutron star structure and the equation of state, Astrophys. J. **550**, 426 (2001).

[91] E. Fonseca *et al.*, Refined mass and geometric measurements of the high-mass PSR J0740 + 6620, Astrophys. J. Lett. **915**, L12 (2021).

[92] O. Benhar and S. Fantoni, *Nuclear Matter Theory*, 1st ed. (CRC Press, Boca Raton, 2020).

[93] See Supplemental Material at http://link.aps.org/supplemental/10.1103/PhysRevLett.128.101101 for a list of the properties of the simulated events.

[94] M. Mapelli and N. Giacobbo, The cosmic merger rate of neutron stars and black holes, Mon. Not. R. Astron. Soc. **479**, 4391 (2018).

[95] T. Dietrich, S. Bernuzzi, and W. Tichy, Closed-form tidal approximants for binary neutron star gravitational waveforms constructed from high-resolution numerical relativity simulations, Phys. Rev. D **96**, 121501(R) (2017).

[96] T. Dietrich *et al.*, Matter imprints in waveform models for neutron star binaries: Tidal and self-spin effects, Phys. Rev. D **99**, 024029 (2019).

[97] L. Wade, J. D. E. Creighton, E. Ochsner, B. D. Lackey, B. F. Farr, T. B. Littenberg, and V. Raymond, Systematic and statistical errors in a Bayesian approach to the estimation of the neutron-star equation of state using advanced gravitational wave detectors, Phys. Rev. D **89**, 103012 (2014).

[98] M. Pitkin, S. Reid, S. Rowan, and J. Hough, Gravitational wave detection by interferometry (ground and space), Living Rev. Relativity **14**, 5 (2011).

[99] G. Ashton *et al.*, BILBY: A user-friendly Bayesian inference library for gravitational-wave astronomy, Astrophys. J. Suppl. Ser. **241**, 27 (2019).

[100] I. M. Romero-Shaw *et al.*, Bayesian inference for compact binary coalescences with BILBY: Validation and application to the first LIGO-Virgo gravitational-wave transient catalogue, Mon. Not. R. Astron. Soc. **499**, 3295 (2020).

[101] S. A. Usman, J. C. Mills, and S. Fairhurst, Constraining the inclinations of binary mergers from gravitational-wave observations, Astrophys. J. **877**, 82 (2019).

[102] H.-Y. Chen, S. Vitale, and R. Narayan, Viewing Angle of Binary Neutron Star Mergers, Phys. Rev. X **9**, 031028 (2019).

[103] R. E. Kass and A. E. Raftery, Bayes factors, J. Am. Stat. Assoc. **90**, 773 (1995).

[104] B. P. Abbott *et al.* (LIGO Scientific, Virgo Collaborations), GWTC-1: A Gravitational-Wave Transient Catalog of Compact Binary Mergers Observed by LIGO and Virgo during the First and Second Observing Runs, Phys. Rev. X **9**, 031040 (2019).

[105] R. Abbott *et al.* (LIGO Scientific, Virgo Collaborations), GWTC-2: Compact Binary Coalescences Observed by LIGO and Virgo During the First Half of the Third Observing Run, Phys. Rev. X **11**, 021053 (2021).

[106] B. P. Abbott *et al.* (LIGO Scientific, Virgo Collaborations), GW170817: Measurements of Neutron Star Radii and Equation of State, Phys. Rev. Lett. **121**, 161101 (2018).

[107] I. Harry and T. Hinderer, Observing and measuring the neutron-star equation-of-state in spinning binary neutron star systems, Classical Quant. Grav. **35**, 145010 (2018).